Cumulant expansion for phonon contributions to the electron spectral function

S. M. Story,[1] J. J. Kas,[1] F. D. Vila,[1] M. J. Verstraete,[2] and J. J. Rehr[1]
[1]*Department of Physics, University of Washington Seattle, Seattle, Washington 98195, USA*
[2]*Institut de Physique, Université de Liège, B-4000 Sart Tilman, Belgium*
(Received 23 July 2014; revised manuscript received 21 October 2014; published 19 November 2014)

We describe an approach for calculations of phonon contributions to the electron spectral function, including both quasiparticle properties and satellites. The method is based on a cumulant expansion for the retarded one-electron Green's function and a many-pole model for the electron self-energy. Pole models are also used for the phonon density of states and the Eliashberg functions. Our calculations incorporate *ab initio* dynamical matrices and electron-phonon couplings from the density functional theory. Illustrative results are presented for several elemental metals and for Einstein and Debye models with a range of coupling constants. These are compared with experiment and other theoretical models. Estimates of corrections to Migdal's theorem are obtained by comparing with leading order contributions to the self-energy, and are found to be significant only for large electron-phonon couplings and low temperatures.

DOI: 10.1103/PhysRevB.90.195135 PACS number(s): 63.20.dk, 07.05.Tp, 71.45.Gm

I. INTRODUCTION

To first approximation, electronic and vibrational properties can be treated separately in condensed matter due to the large mass ratio between electrons and ions, e.g., within the Born-Oppenheimer approximation. However, corrections to this approximation, which depend on the strength of the electron-phonon interaction, are of considerable importance both theoretically and experimentally. Here we investigate the effects of electron-phonon interactions on the quasiparticle properties and inelastic losses of electrons due to coupling to phonons. Due to such interactions, the electron energy levels ε_k are not sharply defined, but have finite lifetimes characterized by the electron self-energy Σ, which lead to broadening of the associated spectral function. In addition, phonon excitations give rise to inelastic losses. Such effects are visible experimentally, e.g., in high resolution ARPES spectra at low temperatures [1].

In general, the electron spectral function at energies near the Fermi level is dominated by a sharp quasiparticle peak, but it can also exhibit satellites due to phonon excitations. According to Migdal's theorem [2], only the leading order electron-phonon interaction contributions to the self-energy are important, due to the large mass ratio between electrons and nuclei. In that case, the electron self-energy can be approximated by the simplest diagram, and vertex corrections can be neglected. We will refer to this diagram as the Migdal approximation (MA). The Migdal approximation (MA) is analogous to the GW approximation of Hedin [3] for electrons coupled to plasmons, where G is the electron Green's function and W the screened Coulomb interaction, by replacing W with the phonon propagator D. This approximation has been investigated in detail [4–8] and extended to finite temperature, e.g., by Allen [9]. The MA leads to a spectral function with a quasiparticle peak and two satellite features originating from single-boson excitations, one on each side of the quasiparticle peak. However, this leading order approximation is generally unsatisfactory as the satellite peaks typically appear at the wrong energies and with the wrong intensities compared to experiment. Moreover, systems of electrons coupled to neutral bosonic excitations typically exhibit multiple satellites [10,11]. Thus it is of interest to investigate possible corrections to Migdal's theorem, i.e., the effects of higher order terms in an expansion in powers of the electron-phonon coupling [12]. One approach to this end is to investigate contributions to the self-energy from the vertex function Γ, as in the formal identity $\Sigma = iGD\Gamma$. However, direct calculations of Γ have been formidably challenging, and there has been little progress along these lines. An attractive alternative that overcomes some of the above shortcomings is provided by the cumulant expansion [12–14], which is an exponential representation of the electron Green's function in the time domain. The cumulant expansion is exact for the case of a deep core level coupled to bosons, and generalizations have been developed for valence electrons coupled to plasmons [15,16]. The approach has been applied with considerable success in cases ranging from multiple plasmon satellites in photoemission [17] to dynamical mean field theory [18]. Nevertheless, the conventional approach based on the time-ordered Green's function is only strictly applicable for the hole *or* particle branch of the spectral function, depending on whether the state is above or below the Fermi level. This limitation is particularly problematic in systems with particle-hole symmetry, such as electrons coupled to phonons. To overcome this difficulty, we utilize here the recently developed retarded cumulant (RC) approach, which is based on a particle/hole cumulant and a *retarded* Green's function formalism [14]. A further goal of the present work is to develop a practical approach for calculations of phonon contributions to properties of condensed matter.

The remainder of this paper is organized as follows. In Sec. II, we describe the retarded cumulant expansion method and many-pole model self-energy used to calculate phonon contributions to the electron spectral function. Section III gives details on how this method is implemented computationally with our workflow tool AI2PS. Finally, our results are presented in Sec. IV, and Sec. V contains a summary and conclusions.

II. THEORY AND METHODOLOGY

In this section, we briefly summarize the Migdal approximation (MA) and retarded cumulant (RC) methods used in

this work for calculations of the electron spectral function. As usual, the Hamiltonian for the many-electron system linearly coupled to phonons can be represented as

$$H = \sum_k \varepsilon_k^0 c_k^\dagger c_k + \sum_q \omega_q a_q^\dagger a_q + \sum_{kk'q} V_{kk'}^q (a_q + a_q^\dagger) c_k^\dagger c_{k'}, \tag{1}$$

where k denotes the electron levels and q the phonon modes with bare energies ε_k^0 and ω_q, respectively, $V_{kk'}^q$ are the electron-phonon matrix elements, and c_k ($c_k^\dagger$) and a_q ($a_q^\dagger$) are the electron and phonon destruction (creation) operators. In this paper, we use atomic units $e = \hbar = m = 1$ and $k_B = 0.08617$ meV/K. At low temperatures, the electrons are nearly degenerate with Fermi energy ε_F and $\omega_q \ll \varepsilon_F \ll \omega_p$, where ω_p is the dominant plasmon excitation energy ($\sim$10 eV) and ε_F is taken relative to the bottom of the band. Thus, for our purposes here, the density of electron states near ε_F is replaced by a constant, which we assume is nonvanishing. The generalization to insulators or molecular systems with discrete spectra near ε_F is straightforward, but will not be treated here.

A. MA spectral function

Briefly, the Migdal approximation for the self-energy is given by $\Sigma = iGD$, where G is the one-electron Green's function and D is the phonon propagator. Within MA, the usual strategy is to calculate the spectral function $A_k(\omega)$ from the imaginary part of the one-electron Green's function in frequency space [4],

$$\begin{aligned} G_k(\omega) &= \frac{1}{\omega - \varepsilon_k^0 - \Sigma_k(\omega)}, \\ A_k(\omega) &= \frac{1}{\pi} |\mathrm{Im}\, G_k(\omega)| \\ &= \frac{1}{\pi} \frac{|\mathrm{Im}\, \Sigma_k(\omega)|}{\left|\omega - \varepsilon_k^0 - \mathrm{Re}\, \Sigma_k(\omega)\right|^2 + |\mathrm{Im}\, \Sigma_k(\omega)|^2}. \end{aligned} \tag{2}$$

The spectral function is comprised of two main features—a dominant quasiparticle peak at $\omega = \varepsilon_k = \varepsilon_k^0 + \Sigma_k$ with width $\mathrm{Im}\, \Sigma_k$ and phonon satellites at $\omega = \varepsilon_F \pm \omega_q$, consistent with Ref. [4]. Other physical properties such as the quasiparticle lifetime and energy levels can be obtained from the properties of $A_k(\omega)$ and $\Sigma_k(\omega)$.

B. RC spectral function

As noted in the Introduction, the conventional time-ordered cumulant expansion must be generalized to treat cases with particle-hole symmetry, such as phonon excitations in metals [12]. Our treatment is based on the RC formalism which is discussed in detail by Kas *et al.* [14]. For a degenerate Fermi system in the absence of plasmons, the RC representation of the retarded one-particle Green's function is

$$\begin{aligned} G_k^R(t) &= G_k^{0,R}(t) e^{C_k^R(t)}, \\ G_k^{0,R}(t) &= -i\, e^{-i\varepsilon_k^0 t} \theta(t), \end{aligned} \tag{3}$$

where $C_k^R(t)$ is the cumulant as described below. Formally, the spectral function is obtained from the Fourier transform of $G_k^R(t)$

$$A_k(\omega) = \mathrm{Im} \int_{-\infty}^{\infty} \frac{dt}{\pi} e^{i\omega t} G_k^R(t). \tag{4}$$

The retarded particle/hole cumulant $C_k^R(t)$ is then approximated by the second order (in electron-phonon coupling) cumulant diagram [14]

$$\begin{aligned} C_k^R(t) &\approx C_{2,k}^R(t) \\ &= i e^{i\varepsilon_k^0 t} \int_{-\infty}^{\infty} \frac{d\omega}{2\pi} e^{-i\omega t} \left[G_k^{0,R}(\omega)\right]^2 \Sigma_k^R(\omega). \end{aligned} \tag{5}$$

This diagram is conveniently evaluated in frequency space [14] and can be expressed in terms of the imaginary part of the $G^0 D^0$ boson excitation spectrum $\beta_k(\omega)$ as

$$C_k^R(t) = \int_{-\infty}^{\infty} d\omega\, \beta_k(\omega) \frac{e^{i\omega t} - i\omega t - 1}{\omega^2}, \tag{6}$$

where $\beta_k(\omega)$ is obtained from the MA self-energy

$$\beta_k(\omega) = \frac{1}{\pi} \left|\mathrm{Im}\, \Sigma_k\left(\omega + \varepsilon_k^0\right)\right|. \tag{7}$$

Consequently, the ingredients in the RC spectral function are similar to those in the MA spectral function and are therefore no more difficult to calculate. Since we approximate the noninteracting Green's function with that of a homogeneous electron gas, material-specific band structure will not be reflected in the resulting spectral functions. In contrast to the conventional time-ordered cumulant expansion, which only contains frequencies within the particle or hole branches, the retarded cumulant in Eq. (6) contains *all* frequencies, and explicitly builds in the particle-hole symmetry desired for phonons. Also, due to the behavior of the self-energy $\Sigma_k(\omega)$ (Fig. 1), multiple phonon satellites may exist with the cumulant expansion, as peaks at integer multiples of ω_E on both sides of the Fermi energy ε_F. This is in contrast to the case with plasmons, where the satellites appear at multiples of ω_p from the quasiparticle peak at ε_k.

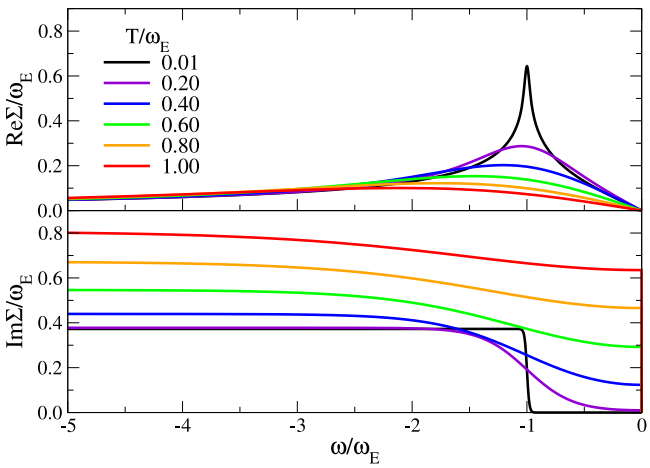

FIG. 1. (Color online) Real (top) and imaginary (bottom) parts of the self-energy $\Sigma_k(\omega)$ in Eq. (9) using the Einstein model for Cu, where $\omega_E = 21.6$ meV $= 251$ K (see text). Positive ω is not shown, as Re Σ and Im Σ and can be determined from the odd parity of $\Sigma_k(\omega)$.

C. Many-pole self-energy

Above we gave the formulas relating the RC and MA spectral functions to the MA self-energy. We now focus on a self-energy model appropriate for phonons. Here we have adapted the finite-temperature Einstein model for phonons [9,19,20], where the self-energy is represented as a sum over Einstein modes. For a single mode with Einstein frequency ω', the MA self-energy at finite temperature T (with unit coupling) is given by [9,20]

$$\Sigma^{\mathrm{E}}(\omega,\omega',T) = -i\pi\left[n(\omega')+\frac{1}{2}\right] + \frac{1}{2}\Psi\left(\frac{1}{2}+i\frac{\omega'-\omega}{2\pi T}\right) - \frac{1}{2}\Psi\left(\frac{1}{2}-i\frac{\omega'+\omega}{2\pi T}\right), \tag{8}$$

where $n(\omega)$ is the Bose-Einstein distribution and $\Psi(z)$ is the digamma function. The electron-phonon coupling constants in the model are represented in terms of the Eliashberg function $\alpha^2 F_k$. The self-energy is then [9,19]

$$\Sigma_k(\omega,T) = \int d\omega' 2\Sigma^{\mathrm{E}}(\omega,\omega',T)\alpha^2 F_k(\omega'). \tag{9}$$

We emphasize that the form of the self-energy in Eq. (9) is strictly appropriate only for cases where the bandwidth of electron states near the Fermi energy is large compared to characteristic phonon energies ω, and will not work for sharp band features. This is the case for valence states in metals and in many semimetals, semiconductors, and insulators, but becomes questionable in the case of small molecules and core level states. Thus in the present work, we focus only on a selection of metallic systems covering a range of electron-phonon couplings. As an example, Fig. 1 shows the real and imaginary parts of the self-energy calculated using Eq. (9) when coupling to a single Einstein mode, i.e., an Einstein model for the phonon spectrum in Cu. We also note that the approximation in Eq. (8) neglects Debye-Waller corrections to the self-energy discussed, for example, by Allen and Heine and others [21–23]. This correction is found to give temperature dependent shifts in the quasiparticle energies and a broadening of the energy bands. On the other hand, this term gives no contribution to the excitation spectrum and hence the structure of the spectral function [21], which is the main topic of this work.

Generally, the Eliashberg function depends on both k and k' through the electron-phonon matrix elements $g^q_{kk'}$ [25–28]. However, since the phonon contributions to the spectral function involve energies very close to ε_F, it is sufficient for our purposes here to use the Eliashberg function averaged over the Fermi surface

$$\alpha^2 F(\omega) = \frac{1}{2\pi N(\varepsilon_F)}\sum_q \sum_{\varepsilon_k,\varepsilon_{k'}\approx\varepsilon_F} \left|g^q_{kk'}\right|^2 \delta(\omega-\omega_q),$$
$$g^q_{kk'} = 2\sum\langle\psi_{k'}|\delta V^q|\psi_k\rangle, \tag{10}$$

where $N(\varepsilon_F)$ is the bare density of states at the Fermi level, δV is the change in potential due to a change in the nuclear

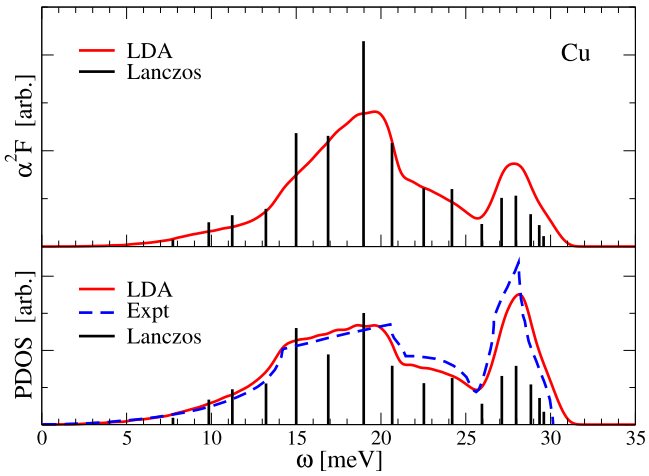

FIG. 2. (Color online) Eliashberg function (top) $\alpha^2 F(\omega)$ and total density of modes (bottom) for Cu at the Fermi level $k = k_F$ obtained from ABINIT with our many-pole approximations α^2_i, F_i calculated by the Lanczos inversion tools in FEFF9 (see text). Experimental PDOS taken from Ref. [24]. Calculated frequencies have been scaled using an overall Grüneisen parameter to match the PDOS peak frequency with experiment.

parameters, and the sum over spin states for nonmagnetic systems considered here gives a factor of 2. Typically, $\alpha^2 F(\omega)$ is rather similar to the total phonon density of states (PDOS) $F(\omega)$ of the system (see Fig. 2), allowing us to express it as a smooth coupling $\alpha^2(\omega)$ multiplying the PDOS. Moreover, it is convenient to use a many-pole model for the PDOS [4], analogous to the plasmon-pole self-energy model of Hedin and Lundqvist [29–32]. The integration over the phonon frequencies ω' in Eq. (9) can then be replaced by a discrete sum over a sufficiently large number of poles without significant loss of accuracy. To this end, an efficient many-pole Lanczos representation of the PDOS has been developed [33],

$$F^{\mathrm{MP}}(\omega) = \sum_i F_i \delta(\omega-\omega_i). \tag{11}$$

Thus a many-pole representation of the Eliashberg function $\alpha^2 F^{\mathrm{MP}}$ can be constructed similarly,

$$\alpha^2 F^{\mathrm{MP}}(\omega) = \sum_i \alpha^2(\omega) F_i \delta\left(\omega-\omega_i\right), \tag{12}$$

where the strength $\alpha^2(\omega)$ is obtained from Eq. (10) and the PDOS $F(\omega)$,

$$\alpha^2(\omega) = \alpha^2 F(\omega)/F(\omega). \tag{13}$$

A 16-pole representation of the copper Eliashberg function is shown in Fig. 2. Finally, an effective or mean electron-phonon coupling constant λ can be defined, which is related to the first inverse frequency moment of the Eliashberg function [34]

$$\lambda = 2\int_0^\infty \frac{d\omega}{\omega}\alpha^2 F(\omega) \approx 2\sum_i \frac{\alpha_i^2 F_i}{\omega_i}. \tag{14}$$

This quantity provides a dimensionless characterization of the strength of electron-phonon coupling in a given material.

III. IMPLEMENTATION

The calculations of phonon properties presented here were carried out using AI2PS (*ab initio* DFT to phonon spectra) [35], a workflow tool we have developed that links density functional theory electronic structure codes, ABINIT in this case [36,37], to the vibrational properties module of real-space Green's function code FEFF9 [38]. AI2PS can be used to calculate phonon properties such as Debye-Waller factors in x-ray spectra. The modular interface automatically coordinates the desired workflow. Briefly, for our purposes here, AI2PS uses ABINIT to generate a set of real-space symmetry-inequivalent blocks of the lattice dynamical matrix (DM), which are used to calculate the many-pole PDOS $F^{\mathrm{MP}}(\omega)$ [33]. The code ABINIT also yields both $F(\omega)$ and $\alpha^2 F(\omega)$, which are used to calculate the couplings $\alpha^2(\omega)$ using Eq. (13). Since Eq. (9) is restricted to energies near the Fermi level, this presently excludes any k-dependent features in the spectral functions presented in the current study. The ABINIT calculations used Troullier-Martins LDA pseudopotentials provided by ABINIT [39], and an energy cutoff of 50 hartree; for convergence of $\alpha^2 F(\omega)$, a $32\times32\times32$ Monkhorst-Pack k-point grid was found to be necessary. For the metallic systems discussed here, the occupation numbers were smeared with the Methfessel and Paxton scheme [40] with a broadening parameter of 0.025. To simplify the numerical calculations by removing self-energy shifts, the RC and MA spectral function expressions were expressed in terms of the quasiparticle energy $\varepsilon_k = \varepsilon_k^0 + \mathrm{Re}\Sigma_k(\varepsilon_k^0)$ as opposed to ε_k^0 [see Eqs. (2), (3), and (7)].

IV. RESULTS AND DISCUSSION

In this section, we present illustrative results for several elemental metals and for Einstein and Debye models with a range of electron-phonon couplings over a range of temperatures and energies for both the RC and MA methods.

A. Einstein model

As a first example, we consider the Einstein model self-energy Σ^{E}, i.e., using the single-pole (zeroth-order Lanczos) approximation for the Eliashberg function,

$$\alpha^2 F(\omega) \to \alpha_E^2 \delta(\omega - \omega_E), \tag{15}$$

where ω_E is the Einstein frequency and $\alpha_E^2 = \alpha^2(\omega_E)$. For realistic systems, the value of ω_E is taken to be the centroid of the calculated PDOS. As an example, we present results for an Einstein model with $\omega_E = 21.6$ meV (251 K), representative of Cu metal, in Fig. 3. Note that phonon satellites in the spectral function are visible only for quasiparticle energies small compared to phonon frequencies $\varepsilon_k - \varepsilon_F < \omega_E$, and very low temperatures ($\sim$10 K), as seen in the top two panels of Fig. 3. For the Einstein model, the mean coupling constant λ is simply $2\alpha_E^2/\omega_E$, so we artificially ramp up the coupling by manually setting the value of α_E^2. Typically, metals have coupling constants λ that range from roughly 0.1 to 1.7 [28], so we will focus on that range. The satellites become larger as λ is increased (third panel), and for $\lambda = 1.6$, a weak second phonon satellite becomes apparent at $\omega = \varepsilon_F \pm 2\omega_E$. The relative weakness of the second satellite even at $\lambda = 1.6$ suggests Migdal's theorem is valid to high accuracy for typical metals, apart from corrections close to the Fermi energy at very low temperatures.

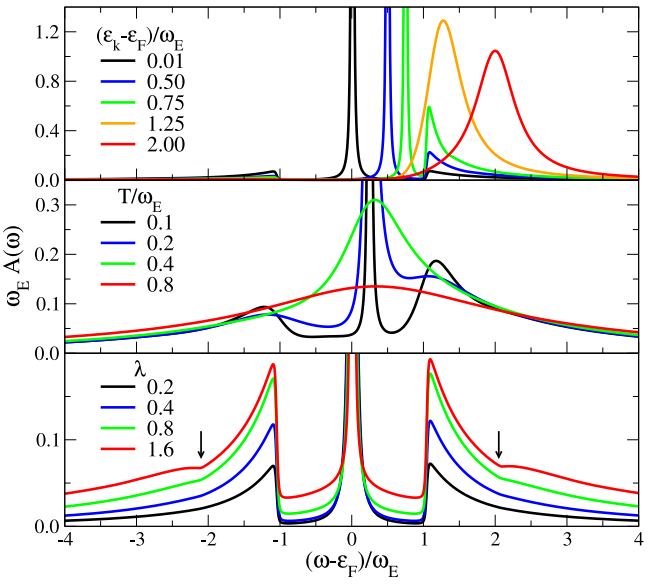

FIG. 3. (Color online) Spectral function for the Einstein model using the RC method, where ω_E is the Einstein energy. Top: varying quasiparticle energy for low temperature and weak coupling ($T = 0.01\omega_E$; $\lambda = 0.2$); middle: varying temperature near the Fermi energy and with medium coupling ($\varepsilon_k - \varepsilon_F = 0.25\omega_E$; $\lambda = 1.0$); bottom: varying electron-phonon coupling constant at low temperature near the Fermi energy ($\varepsilon_k - \varepsilon_F = T = 0.01\omega_E$).

B. Debye model

For comparison, we show similar results using the Debye model PDOS converted to a many-pole form in Fig. 4, with quantities expressed in terms of the Debye temperature for copper $\Theta_D = 315$ K $= 27.1$ meV $= \omega_D$. Overall, the Debye model shows trends quite similar to the Einstein model. However, the phonon satellites are not as sharply peaked, and the satellites at $\varepsilon_F \pm 2\omega_D$ are indiscernible at the same scale for $\lambda = 1.6$. Note that artifacts of the many-pole model can be seen in the spectral functions as small peaks near the Fermi energy (third panel), though these effects are negligible compared to the phonon satellites.

C. Comparison of RC and MA

We note that the electron spectral function near the Fermi level ε_F is generally nearly symmetrical due to particle-hole symmetry, and is sensitive to phonon correlations beyond MA at strong electron-phonon coupling, as illustrated by the significant deviation of RC from MA seen in Fig. 5. Thus it is useful to compare the RC and MA methods in this limit, especially since the differences characterize corrections to the Migdal approximation due to vertex effects. Figure 5 shows that the two methods differ significantly at strong couplings *and* low temperatures compared to the Debye or Einstein temperature (see Table I for distribution of spectral weight). The RC method gives larger satellite weights, with a stronger first satellite peak closer to the expected $\varepsilon_F \pm \omega_E$ (see inset to Fig. 5). However, the differences between the

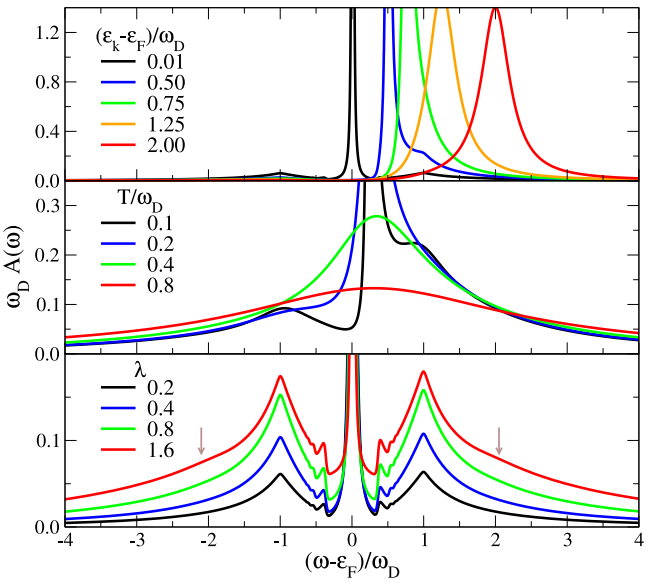

FIG. 4. (Color online) Spectral function for the Debye model using the RC method, where ω_D is energy corresponding to the Debye temperature. Top: varying quasiparticle energy for low temperature and weak coupling ($T = 0.01\omega_D$; $\lambda = 0.2$); middle: varying temperature near the Fermi energy and with medium coupling ($\varepsilon_k - \varepsilon_F = 0.25\omega_D$; $\lambda = 1.0$); bottom: varying electron-phonon coupling constant at low temperature near the Fermi energy ($\varepsilon_k - \varepsilon_F = T = 0.01\omega_D$).

two methods diminish as the temperature is increased towards room temperature. Neither method shows a noticeable two phonon satellite peak.

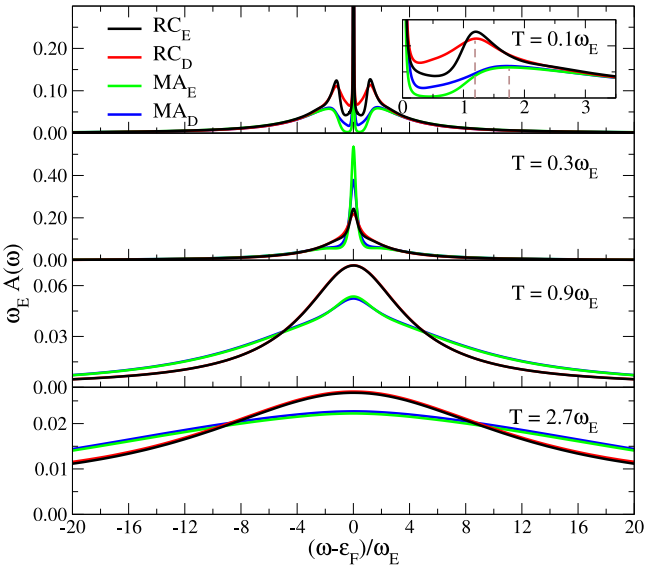

FIG. 5. (Color online) Comparison of spectral function from the RC and MA methods using the Einstein and Debye models at strong coupling (i.e., $\lambda = 1.6$) near the Fermi level ($\varepsilon_k = \varepsilon_F + 0.01\omega_E$) for various temperatures, where $\omega_D \approx 1.3\omega_E$. Inset: enlarged view of phonon satellites seen in the top panel. Note the satellite peak for the MA method is farther out.

TABLE I. Comparison of spectral weights for the quasiparticle peak, hole satellite, and particle satellite (Z_k, w_h, w_p, respectively) using the RC and MA methods, done for the Einstein/Debye models at large coupling ($\lambda = 1.6$) and several elemental metals near the Fermi level at low temperature ($\varepsilon_k = \varepsilon_F + 0.01\omega_{E,\mathrm{Cu}} = 0.216$ meV; $T = 0.1\omega_{E,\mathrm{Cu}} = 25.1$ K).

		Z_k	w_h	w_p	λ
RC	Einstein	0.19	0.39	0.42	1.60
	Debye	0.18	0.39	0.43	1.60
	V	0.29	0.34	0.37	1.17
	Nb	0.31	0.33	0.36	1.08
	Pb	0.35	0.31	0.34	0.95
	Ta	0.37	0.30	0.33	0.91
	Cu	0.85	0.07	0.08	0.16
MA	Einstein	0.38	0.31	0.31	1.60
	Debye	0.37	0.31	0.32	1.60
	V	0.45	0.27	0.28	1.17
	Nb	0.46	0.27	0.27	1.08
	Pb	0.49	0.25	0.26	0.95
	Ta	0.50	0.24	0.26	0.91
	Cu	0.86	0.07	0.07	0.16

D. Selected metals: Cu, Nb, Pb, Ta, and V

Next, we present results for the spectral function for a few elemental solids (Fig. 6) representative of a range of electron-phonon couplings (see Table II). To obtain the full spectral function for these materials, we use the Lanczos many-pole representation of Eq. (12), as shown in Fig. 2 for copper. The results for these metals using either method follow general trends similar to the Einstein and Debye models. Copper, which has a relatively weak coupling ($\lambda \sim$

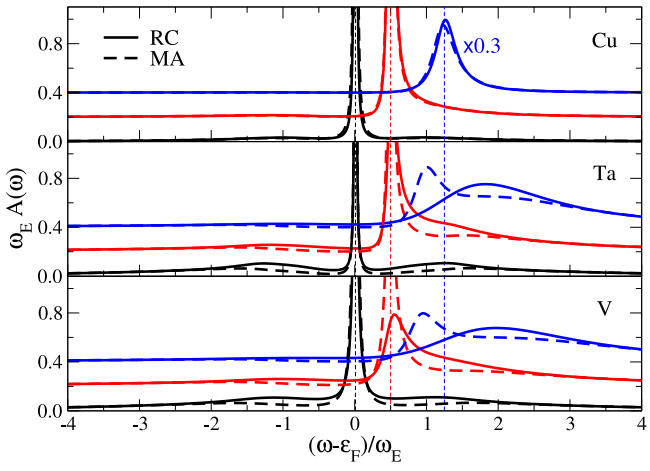

FIG. 6. (Color online) Comparing the spectral functions of the RC and MA methods for select metals at low temperature and three quasiparticle energies ε_k for $(\varepsilon_k - \varepsilon_F)/\omega_E = 0.01, 0.5, 1.25$ (bottom, middle, top vertically offset curves respectively in each panel, with arrows indicating corresponding location along the horizontal axis). For Cu, Ta, and V, $\omega_E = 21.6$, 15.0, and 24.1 meV, respectively, and $T = 0.15\omega_E = 37.65$, 17.4, and 42.0 K, respectively. The spectral function for Cu with $\varepsilon_k - \varepsilon_F = 1.25\omega_E$ has been scaled vertically to fit, as indicated.

TABLE II. Calculated electron-phonon coupling constants using two methods—the inverse moment of the many-pole $\alpha^2F(\omega)$ [Eq. (14)] and the temperature dependence of the quasiparticle linewidth taken from the spectral functions at large ε_k—and experimental results for comparison.

	λ^{MP}	λ^{Γ}		λ^{expt}	
V	1.174	0.899	0.82[b]	1.09[c]	0.80[d]
Nb	1.079	0.897	1.04[b]	1.06[c]	1.16[d]
Pb	0.946	0.955	1.55[b]	1.48[c]	1.45[d]
Ta	0.909	0.809	0.78[b]	0.87[c]	
Cu	0.155	0.126	0.10[a]	0.13[c]	0.08[d]

[a]Reference [41].
[b]Reference [42].
[c]Reference [43].
[d]Reference [44].

0.1), displays near agreement between the RC and MA methods. Tantalum and vanadium, on the other hand, have medium to strong couplings, respectively, and show significant differences between the two methods. Most noticeably, for increasing quasiparticle energies, both the distribution of weight between the quasiparticle and satellites and the location of these peaks disagree significantly, possibly enough to be noticeable experimentally. However, these differences can only be seen at low temperatures (∼50 K). Even with the strongest coupling, vanadium does not show multiple phonon satellites, indicating Migdal's theorem is valid to high accuracy for phonons in these materials.

E. Comparison with experiment

Evidence for electron-phonon effects in the spectral function have been measured in a number of cases. For instance, the value of the mean coupling constant λ can be obtained experimentally from the slope of the quasiparticle linewidth $\Gamma \sim 2\pi\lambda k_B T$ versus temperature [19]. Thus calculations of quasiparticle linewidths characterize the phonon contributions to the quasiparticle broadening. Our calculated quasiparticle peak FWHM (Fig. 7) are comparable to those measured experimentally [45–47]. As an example, we find a slope of 0.0680 meV/K for copper at large ε_k (top panel Fig. 7), corresponding to $\lambda = 0.126$. Due to the redistribution of spectral weight from the quasiparticle peak to the phonon satellites for $\varepsilon_k \sim \varepsilon_F$ (lower panel Fig. 7), the temperature trends are significantly steeper, resulting in inflated λ values. The λ taken from the large ε_k calculations are more consistent with experimental observations, and are listed in Table II. The calculated λ for the metals using Eq. (14) are given as well in Table II , along with several experimental results for comparison. Overall, there is decent agreement with experiment. The heavier metals show more discrepancy, which is likely an effect of the absence of spin-orbit coupling in our simulations [48,49].

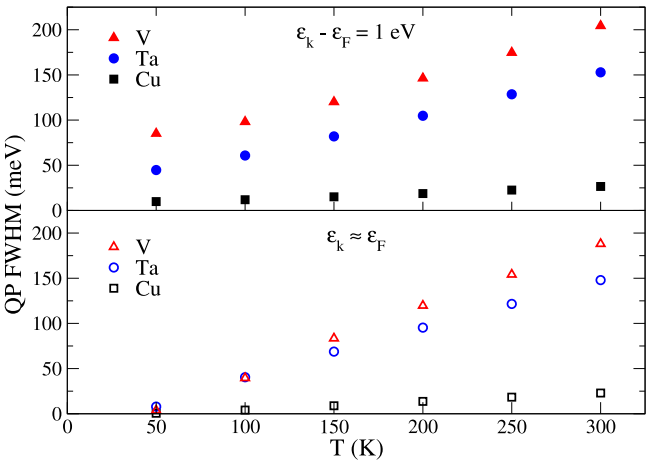

FIG. 7. (Color online) Quasiparticle peak width versus temperature at the Fermi energy $\varepsilon_k = \varepsilon_F$ (bottom), and at moderate quasiparticle energy $\varepsilon_k = \varepsilon_F + 1.0$ eV (top) for Cu, Ta, and V. The linear relationship, given by $\Gamma \sim 2\pi\lambda k_B T$, gives an estimate of the electron-phonon coupling strength λ. Table II shows λ derived from the $\varepsilon_k = \varepsilon_F + 1.0$ eV calculations, to limit any skewing of the quasiparticle widths due to phonon satellites.

V. SUMMARY AND CONCLUSIONS

We have implemented a retarded cumulant (RC) expansion approach to calculate phonon contributions to electron spectral function. This approach goes beyond the standard Migdal approximation (MA) to include effects of phonon excitation satellites in the electron spectral function. Our calculations show that the phonon contribution to the quasiparticle peak is linearly dependent on temperature. We verify that Migdal's theorem is generally satisfied for phonons to high accuracy. Thus the effects of vertex corrections lead to deviations between the MA and RC approaches and multiple satellites in the spectral function and are generally negligible except at very low T ($T \lesssim 50$ K) and very strong electron-phonon couplings ($\lambda \gtrsim 1$), and would require roughly meV resolution to discern experimentally. With an appropriate self-energy, the method presented here can also be extended to treat insulators and molecular systems.

ACKNOWLEDGMENTS

We thank C. Draxl, L. Reining, P. B. Allen, G. Rignanese, X. Gonze, M. Bernardi, and K. Jorissen for useful discussions, and S. R. Williams and J. Vinson for assistance in code development. The ABINIT code is a common project of the Université Catholique de Louvain, Corning Incorporated and other contributors (see http://www.abinit.org). This work was supported in part by DOE Grant No. DE-FG02-03ER15476.

[1] T. Cuk, D. H. Lu, X. J. Zhou, Z. X. Shen, T. P. Devereaux, and N. Nagaosa, Phys. Status Solidi B **242**, 11 (2005).
[2] A. B. Migdal, Sov. Phys. JETP **7**, 996 (1958).
[3] L. Hedin, J. Phys.: Condens. Matter **11**, R489 (1999).

[4] S. Engelsberg and J. R. Schrieffer, Phys. Rev. **131**, 993 (1963).
[5] M. Bernardi, M. Palummo, and J. C. Grossman, Nano Lett. **13**, 3664 (2013).
[6] D. Y. Qiu, F. H. da Jornada, and S. G. Louie, Phys. Rev. Lett. **111**, 216805 (2013).
[7] M. S. Hybertsen and S. G. Louie, Phys. Rev. B **34**, 5390 (1986).
[8] G. Onida, L. Reining, and A. Rubio, Rev. Mod. Phys. **74**, 601 (2002).
[9] P. B. Allen and B. Mitrović, in *Solid State Physics*, edited by H. Ehrenreich, F. Seitz, and D. Turnbull (Academic Press, New York, 1982), Vol. 37, pp. 1–92.
[10] P. Steiner, H. Höchst, S. Hüfner, L. Ley, and M. Cardona, Top. Appl. Phys. **27**, 349 (1979).
[11] F. Offi, W. Werner, M. Sacchi, P. Torelli, M. Cautero, G. Cautero, A. Fondacaro, S. Huotari, G. Monaco, G. Paolicelli *et al.*, Phys. Rev. B **76**, 085422 (2007).
[12] O. Gunnarsson, V. Meden, and K. Schönhammer, Phys. Rev. B **50**, 10462 (1994).
[13] R. Kubo, J. Phys. Soc. Jpn. **17**, 1100 (1962).
[14] J. J. Kas, J. J. Rehr, and L. Reining, Phys. Rev. B **90**, 085112 (2014).
[15] L. Hedin, Phys. Scr. **21**, 477 (1980).
[16] F. Aryasetiawan, L. Hedin, and K. Karlsson, Phys. Rev. Lett. **77**, 2268 (1996).
[17] M. Guzzo, G. Lani, F. Sottile, P. Romaniello, M. Gatti, J. J. Kas, J. J. Rehr, M. G. Silly, F. Sirotti, and L. Reining, Phys. Rev. Lett. **107**, 166401 (2011).
[18] M. Casula, A. Rubtsov, and S. Biermann, Phys. Rev. B **85**, 035115 (2012).
[19] G. Grimvall, *The Electron-phonon Interaction in Metals* (North-Holland, Amsterdam, 1981).
[20] A. Eiguren and C. Ambrosch-Draxl, Phys. Rev. Lett. **101**, 036402 (2008).
[21] P. B. Allen and V. Heine, J. Phys. C **9**, 2305 (1976).
[22] P. B. Allen and M. Cardona, Phys. Rev. B **23**, 1495 (1981).
[23] P. B. Allen and M. Cardona, Phys. Rev. B **27**, 4760 (1983).
[24] R. M. Nicklow, G. Gilat, H. G. Smith, L. J. Raubenheimer, and M. K. Wilkinson, Phys. Rev. **164**, 922 (1967).
[25] W. L. McMillan, Phys. Rev. **167**, 331 (1968).
[26] G. Grimvall, Phys. Kondens. Mater. **11**, 279 (1970).
[27] P. B. Allen, Phys. Rev. B **6**, 2577 (1972).
[28] S. Y. Savrasov and D. Y. Savrasov, Phys. Rev. B **54**, 16487 (1996).
[29] L. Hedin and S. Lundqvist, Solid State Physics **23**, 1 (1970).
[30] B. I. Lundqvist, Phys. Kondens. Mater. **6**, 193 (1967).
[31] B. I. Lundqvist, Phys. Kondens. Mater. **6**, 206 (1967).
[32] J. J. Kas, A. P. Sorini, M. P. Prange, L. W. Cambell, J. A. Soininen, and J. J. Rehr, Phys. Rev. B **76**, 195116 (2007).
[33] F. D. Vila, J. J. Rehr, H. H. Rossner, and H. J. Krappe, Phys. Rev. B **76**, 014301 (2007).
[34] P. B. Allen, in *Handbook of Superconductivity*, edited by C. P. Poole (Academic Press, New York, 1999), Chap. 9, pp. 478–483.
[35] See http://www.feffproject.org/.
[36] X. Gonze, J.-M. Beuken, R. Caracas, F. Detraux, M. Fuchs, G.-M. Rignanese, L. Sindic, M. Verstraete, G. Zerah, F. Jollet, M. Torrent, A. Roy, M. Mikami, Ph. Ghosez, J.-Y. Raty, and D.C. Allan, Comput. Mater. Sci. **25**, 478 (2002).
[37] X. Gonze, G.-M. Rignanese, M. Verstraete, J.-M. Beuken, Y. Pouillon, R. Caracas, F. Jollet, M. Torrent, G. Zerah, M. Mikami, Ph. Ghosez, M. Veithen, J.-Y. Raty, V. Olevano, F. Bruneval, L. Reining, R. Godby, G. Onida, D. R. Hamann, and D. C. Allan, Z. Kristallogr. **220**, 558 (2005).
[38] J. J. Rehr, J. J. Kas, F. D. Vila, M. P. Prange, and K. Jorissen, Phys. Chem. Chem. Phys. **12**, 5503 (2010).
[39] See http://www.abinit.org/.
[40] M. Methfessel and A. T. Paxton, Phys. Rev. B **40**, 3616 (1989).
[41] P. Chaikin, G. Arnold, and P. Hansma, J. Low Temp. Phys. **26**, 229 (1977).
[42] E. L. Wolf, *Principles of Electron Tunneling Spectroscopy* (Oxford University Press, New York, 1985).
[43] P. B. Allen, Phys. Rev. B **36**, 2920 (1987).
[44] S. D. Brorson, A. Kazeroonian, J. S. Moodera, D. W. Face, T. K. Cheng, E. P. Ippen, M. S. Dresselhaus, and G. Dresselhaus, Phys. Rev. Lett. **64**, 2172 (1990).
[45] B. A. McDougall, T. Balasubramanian, and E. Jensen, Phys. Rev. B **51**, 13891 (1995).
[46] A. Eiguren, B. Hellsing, F. Reinert, G. Nicolay, E. V. Chulkov, V. M. Silkin, S. Hüfner, and P. M. Echenique, Phys. Rev. Lett. **88**, 066805 (2002).
[47] F. Reinert, B. Eltner, G. Nicolay, D. Ehm, S. Schmidt, and S. Hüfner, Phys. Rev. Lett. **91**, 186406 (2003).
[48] M. J. Verstraete, M. Torrent, F. Jollet, G. Zérah, and X. Gonze, Phys. Rev. B **78**, 045119 (2008).
[49] R. Heid, K. P. Bohnen, I. Y. Sklyadneva, and E. V. Chulkov, Phys. Rev. B **81**, 174527 (2010).